

Electronic Supplementary Information

**Ligase detection reaction amplification-activated CRISPR-Cas12a for single-molecule counting of FEN1 in breast cancer tissues**

Zi-yue Wang,<sup>a,†</sup> Shuang-qian Teng,<sup>a,†</sup> Ning-ning Zhao,<sup>a,†</sup> Yun Han,<sup>b</sup> Dong-ling Li,<sup>b</sup> and Chun-yang Zhang<sup>\*,b</sup>

<sup>a</sup> College of Chemistry, Chemical Engineering and Materials Science, Shandong Normal University, Jinan 250014, China.

<sup>b</sup> School of Chemistry and Chemical Engineering, Southeast University, Nanjing 211189, China.

† These authors contributed equally to this work.

\* Corresponding authors. E-mail: zhangcy@seu.edu.cn.

## 1 EXPERIMENTAL SECTION

### 1.1 Chemicals and materials

All HPLC-purified oligonucleotides (Table S1) were synthesized by Sangon Biotechnology Co. Ltd. (Shanghai, China). Thermostable flap endonuclease 1 (FEN1), 10 × ThermoPol reaction buffer (200 mM Tris-HCl, 100 mM (NH<sub>4</sub>)<sub>2</sub>SO<sub>4</sub>, 100 mM KCl, 20 mM MgSO<sub>4</sub>, 1% Triton-X-100, pH 8.8), bovine serum albumin (BSA), EnGen Lba Cas12a, 10 × NEBuffer 2.1 (500 mM NaCl, 100 mM Tris-HCl, 100 mM MgCl<sub>2</sub>, and 1 mg/mL BSA, pH 7.9), exonuclease I (Exo I), exonuclease III (Exo III), lambda exonuclease, and T4 DNA ligase were purchased from New England Biolabs (Ipswich, MA, USA). Ampligase® DNA ligase and Ampligase® 10 × reaction buffer (200 mM Tris-HCl, 250 mM KCl, 100 mM MgCl<sub>2</sub>, 5 mM NAD, and 0.1% Triton® X-100, pH 8.3) were obtained from Epicenter Technologies (Madison, WI, U.S.A.). RNase inhibitor was bought from TaKaRa Bio. Inc. (Dalian, China). Aurintricarboxylic acid (ATA) was obtained from Sigma-Aldrich (St. Louis, MO, USA). Human breast cancer cell line (MCF-7 cells), human cervical carcinoma cell line (HeLa cells), human lung adenocarcinoma cell line (A549 cells) and hepatic normal cells (LO2) were purchased from the Cell Bank of Chinese Academy of Sciences (Shanghai, China). Diethylpyrocarbonate (DEPC)-treated water (RNase free) was purchased from Beyotime Biotechnology Co. Ltd. (Shanghai, China). All other reagents were of analytical grade and used without further purification. The Formalin-fixed paraffin-embedded (FFPE) breast tissue sections were obtained from the Affiliated Hospital of Weifang Medical University (Weifang, Shandong, China), and the experiments were approved by the ethics committee of the Affiliated Hospital of Weifang Medical University. Ultrapure water was prepared by a Millipore filtration system (Millipore, Milford, MA, USA).

**Table S1.** Sequences of the oligonucleotides <sup>a</sup>

note	Sequence (5'-3')
S1	GCC CAT CAA TAT CGA ATA GTC
Cy5-labeled S1	Cy5-GCC CAT CAA TAT CGA ATA GTC
S2	GGG GGG GGC TGA CTA CAA CTT AAA
S3 (S3-22nt)	TTT AAG TTG TAG TCA GAC TAT TCG ATA TTG ATG GGC
X	P-ACT ATT CGA TAT TGA TG*G* G*C
Y	TTT AAG TTG TAG TCA G
Probe X-Y	TTT AAG TTG TAG TCA GAC TAT TCG ATA TTG ATG *G* G*C
crRNA	UAG AUG UUG UCA UCU UUC CAA UCG AAU AGU CUG ACU ACA ACU
Signal probe	FAM-TTATT-BHQ
S3-6 nt	TTC GAT ATT GAT GGG C
S3-10 nt	ACT ATT CGA TAT TGA TGG GC
S3-14 nt	TCA GAC TAT TCG ATA TTG ATG GGC
S3-18 nt	GTA GTC AGA CTA TTC GAT ATT GAT GGG C
ncDNA	GCC CAT CAA TAT CGA ATA GTC TGA CTA CAA CTT AAA

<sup>a</sup> In probe X, the “P” indicates the phosphate group, and “\*” indicates the phosphate group.

## 1.2 Cell culture and preparation of cell extracts

Different cell lines including MCF-7 cells, Hela cells, A549 cells and LO2 cells were cultured in Dulbecco’s modified Eagle’s medium (DMEM) supplemented with 10% fetal bovine serum and 1% penicillin-streptomycin at 37 °C under a 5% CO<sub>2</sub> atmosphere. The cell extracts were prepared using

a nuclear extract kit (Sangon Biotechnology Co. Ltd. (Shanghai, China)) according to the manufacturer's protocol. The obtained supernatant fraction was subjected to FEN1 assay.

### **1.3 FEN1-induced cleavage reaction**

10  $\mu$ L of reaction solution containing 100 nM S1, 100 nM S2, 100 nM S3, and 1  $\times$  ThermoPol reaction buffer (20 mM Tris-HCl, 10 mM  $(\text{NH}_4)_2\text{SO}_4$ , 10 mM KCl, 2 mM MgSO<sub>4</sub>, 0.1% Triton-X-100, pH 8.8) was incubated at 95 °C for 5 min, and then cooled to room temperature to obtain a triplex DNA with a 5'-flap. Then, 5  $\mu$ L of the above reaction products was added into 10  $\mu$ L of reaction system containing 1  $\times$  ThermoPol reaction buffer and different-concentration FEN1, followed by incubation for 30 min at 65 °C.

### **1.4 Ligation-mediated cyclic LDR reaction.**

The ligation reaction was carried out in 10  $\mu$ L of reaction mixture containing 8  $\mu$ L of FEN1-induced cleavage reaction products, 2.5 U of Ampligase® DNA ligase, and 1  $\times$  Ampligase® reaction buffer at 45 °C for 10 min. Then the LDR reaction was carried out in 20  $\mu$ L of reaction mixture containing 10  $\mu$ L of ligation reaction products, 160 nM probe X, 160 nM probe Y, 5 U of Ampligase® DNA ligase, and 1  $\times$  Ampligase® reaction buffer. Subsequently, the mixture was implemented with 40 thermal cycles at 45 °C for 2 min, 95 °C for 30 s. After LDR reaction, 50 U of exonuclease I (Exo I) and 10  $\times$  Exo I reaction buffer were added into the reaction mixture, followed by incubation at 37 °C for 20 min to digest the excess probes Y. The digestion reaction was terminated by incubation at 90 °C for 10 min.

### **1.5 CRISPR-Cas12a-mediated cleavage reaction**

The 20  $\mu$ L of reaction solution containing 10  $\mu$ L of LDR reaction products, 1  $\mu$ M signal probe, 80 nM crRNA, 1  $\times$  NEBuffer 2.1, and 50 nM Cas12a was incubated for 50 min at 37 °C, followed by termination for 10 min at 65 °C.

### **1.6 Single-molecule imaging.**

A total internal reflection fluorescence (TIRF) microscope (Nikon, Ti-E, Japan) was employed for single-molecule imaging. After 10000-fold dilution, 10  $\mu$ L of reaction products was dropped on a glass coverslip for imaging with a sapphire 488-nm laser as the excitation source. An Andor iXon DU897 electron-multiplying charge-coupled device was used to collect the photons. An EMCCD camera (Hamamatsu Photonics K.K., Japan) was employed to acquire the fluorescence images with an exposure time of 500 ms. ImageJ software was employed to count FAM molecules in the region of interest of 600  $\times$  600 pixels, and the average of 9 frames counting was used for data analysis.

### **1.7 Fluorescence measurements.**

Fluorescence emission spectra were recorded by using a FLS1000 photoluminescence spectrometer (Edinburgh Instruments Ltd., Livingston, UK) with both the emission and excitation slits of 5 nm. The excitation wavelength was 488 nm. The FAM fluorescence intensity at 523 nm was used for data analysis.

### **1.8 Gel electrophoresis**

The FEN1-induced cleavage products were analyzed by 16% denaturing polyacrylamide gel (PAGE) in 1  $\times$  TBE buffer (89 mM Tris, 89 mM Boric acid, 2 mM EDTA, pH 8.0) at a 110 V constant voltage for 55 min at room temperature. The gel was stained by SYBR Gold and scanned by using a Bio-Rad ChemiDoc imaging system (California, USA). The ligation products of LDR reaction

were examined by 16% PAGE at a 110 V constant voltage for 55 min at room temperature. The SYBR Gold signal was visualized by using an illumination source of Epi-blue (460–490 nm excitation) and a 518–546 nm filter. The Cy5 signal was visualized by using an illumination source of Epi-red (625–650 nm excitation) and a 675–725 nm filter. The target-activated cleavage of the signal probe products was analyzed by 12% nondenaturing PAGE in 1 × TBE buffer at a 110 V constant voltage for 30 min at room temperature. The FAM signals were visualized by using an illumination source of Epi-blue (460–490 nm excitation) and a 518–546 nm filter.

### **1.9 FEN1 inhibition assay**

For inhibition assay, various-concentration ATA was incubated with 16 U of FEN1 at 65 °C for 5 min, followed by incubation with the enzyme reaction mixture at 65 °C for 30 min. The relative activity (*RA*) of FEN1 was measured according to equation 1.

$$RA = \frac{N_t - N_0}{N_t} \times 100\% \quad (1)$$

where  $N_t$  represents the FAM counts in the presence of FEN1,  $N_i$  represents the FAM counts in the presence of FEN1 + ATA inhibitor, and  $N_0$  represents the FAM counts in the absence of FEN1. The IC<sub>50</sub> value of inhibitor was obtained from the curve-fitting equation.

## **2 SUPPLEMENTARY RESULTS**

### **2.1 Working mechanism of CRISPR-Cas12a system**

The working mechanism of double stranded DNA (dsDNA) as an activator binding to crRNA to initiate CRISPR-Cas12a includes the following steps (Fig. S1A)<sup>1</sup> : (1) CRISPR protein combines crRNA to form a Cas12a-crRNA complex; (2) Cas12a-crRNA complex recognizes the protospacer-adjacent motif (PAM) sequence of target dsDNA (target strand (TS) and non-target strand (NTS))<sup>2</sup>;

(3) the Cas12a serves as a DNA helicase, unwinding target dsDNA to create a triple-strand crRNA-DNA hybrid R-loop; (4) then the crRNA-TS can continually hybridize, resulting in the formation of complete R-loop to induce a conformational change and activation in Cas12a RuvC active domain;<sup>1</sup> (5) subsequently, PAM-distal TS-NTS duplex successively enters the activated RuvC active domain, resulting in cis-cleavage of NTS and TS;<sup>3</sup> (6) Cas12a uses a single RuvC nuclease domain to cleave both strands of target DNA, generating PAM-distal DSBs with larger (5–7 nt) 5' overhangs. The PAM-distal dsDNA is released, and the PAM-proximal dsDNA remains bound to the Cas12a-crRNA complex. Cas12a maintained in a catalytically activated conformation<sup>4</sup> can activate trans-cleavage activity to indiscriminately cleave the nearby non-target single-stranded DNA (ssDNA).<sup>5</sup>

The working mechanism of ssDNA as an activator binding to crRNA to initiate CRISPR-Cas12a includes the following steps (Fig. S1B)<sup>1</sup>: (1) CRISPR protein combines crRNA to form a Cas12a-crRNA complex; (2) Cas12a-crRNA complex recognizes target ssDNA to induce a conformational change and activation of RuvC active domain; (3) Cas12a possesses sequence-independent DNase activity that can cleave non-target single-stranded DNA.<sup>6</sup>

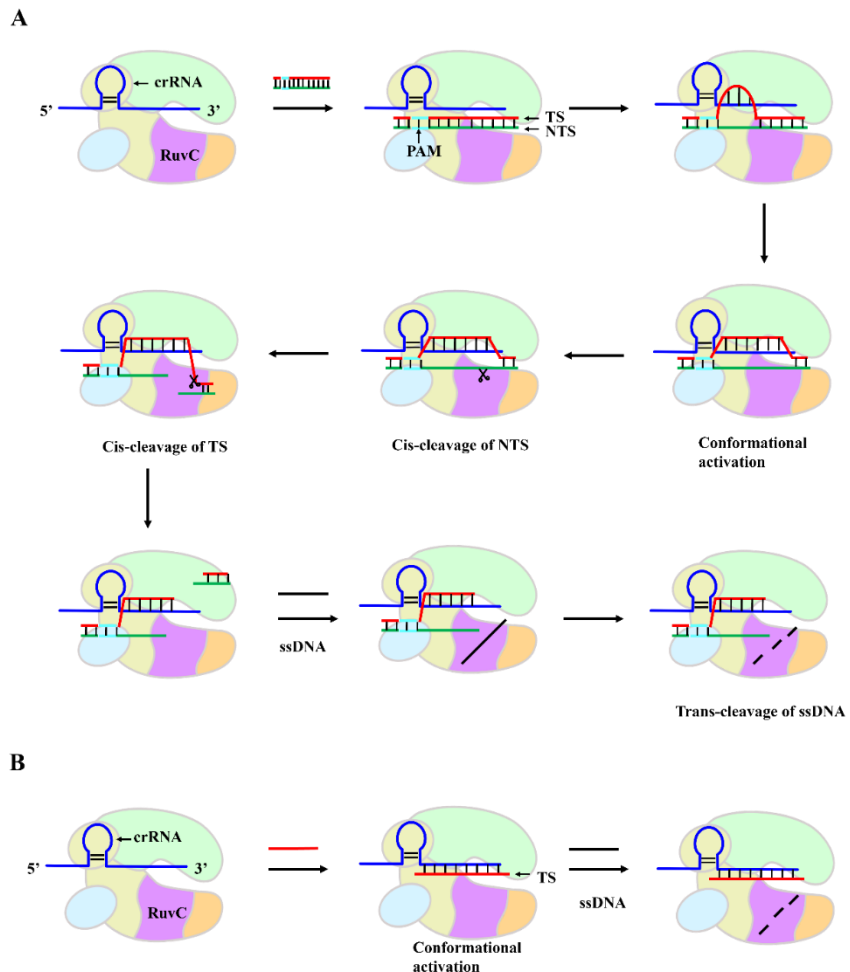


**Fig. S1** (A) Working mechanism of dsDNA as an activator binding to crRNA to initiate CRISPR-Cas12a process. (B) Working mechanism of ssDNA as an activator binding to crRNA to initiate CRISPR-Cas12a process.<sup>1</sup>

## 2.2 Comparison of the performance of Cas12a-crRNA-dsDNA with Cas12a-crRNA-ssDNA

To compare the performance of Cas12a-crRNA-dsDNA with Cas12a-crRNA-ssDNA, we investigated the cleavage activity of CRISPR-Cas12a using various activators including a noncomplementary strand (ncDNA), PAM-contained dsDNA, and ssDNA. As shown in Fig. S2, in the presence of reaction buffer (control, gray column) and ncDNA (green column), negligible fluorescence signal is detected, suggesting that the cleavage activity of cas12a is not activated.

Notably, a high fluorescence signal is observed in target ssDNA (red column) compared with the dsDNA target (blue column). Therefore, we choose ssDNA in combination with crRNA to initiate CRISPR-Cas12a system in this assay.

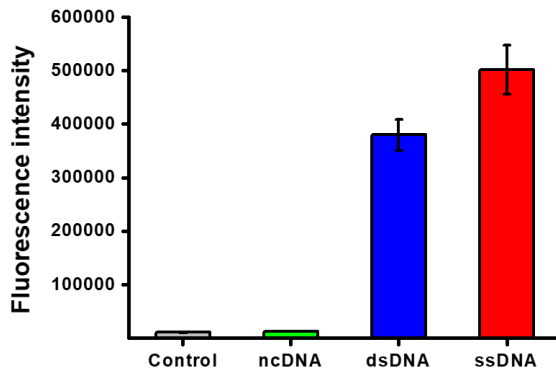


**Fig. S2.** Fluorescence intensity generated by reaction buffer (control, gray column), ncDNA (green column), dsDNA target (blue column), and ssDNA target (red column), respectively. Error bar represents the standard deviation of three independent experiments.

### 2.3 Investigation of the length of activators is bound to crRNA

To guarantee that ssDNA activator in combination with Cas12a-crRNA can achieve the best assay performance, we investigated the influence of the activator length upon the assay performance.<sup>7</sup> We designed five activators bound to crRNA with the length ranging from 6 to 22 nt (Table S1, S3-6 nt, S3-10 nt, S3-14 nt, S3-18 nt, and S3-22 nt). As shown in Fig. S3A, only probe S3-22 nt can produce a significant signal (Fig. S3A, red column), illustrating that 22 nt activator (i.e., bound to crRNA with a length of 22 nt) can effectively activate the cleavage activity of Cas12a.

To demonstrate that individual probe X cannot activate the cleavage activity of Cas12a in the control group, we employed probe X and ligated probe X-Y as the activators to detect the fluorescence signal. As shown in Fig. S3B, individual probe X (the crRNA binding length is only

10 nt, Fig. S3B, 1, orange column) cannot produce a distinct fluorescence signal, because the crRNA binding length is too short (Fig. S3A) to combine with Cas12a-crRNA. On the contrary, the ligated X-Y probe (Fig. S3B, 2, purple column) produces a high fluorescence signal, suggesting that ligated probe X-Y as an activator can effectively activate the cleavage activity of Cas12a.

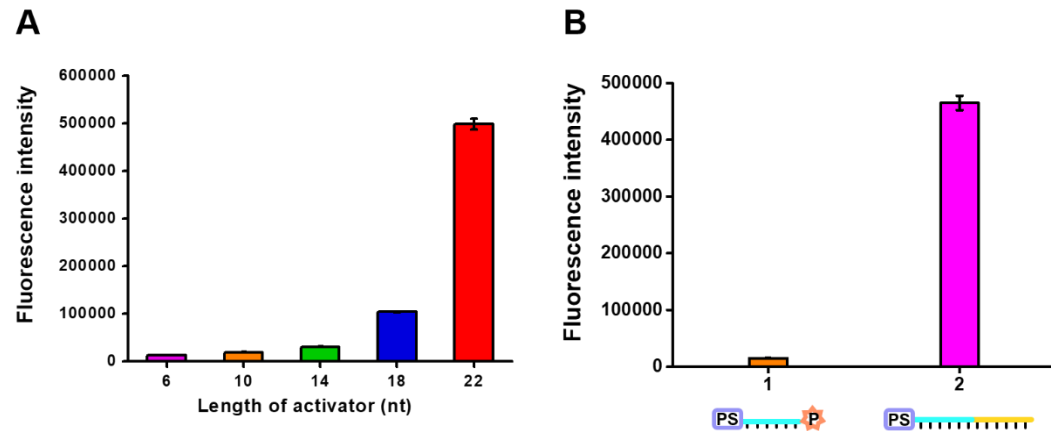


**Fig. S3** (A) Fluorescence intensity generated by different lengths of activators bound to crRNA with a length ranging from 6 to 22 nt. (B) Fluorescence intensity generated by individual X probe (1, orange column) and ligated probe X-Y (2, purple column). Error bar represents the standard deviation of three independent experiments.

#### 2.4 Optimization of reaction temperature and reaction time of FEN1

The reaction temperature and reaction time of FEN1 directly affect the cleavage efficiency. As shown in Fig. S4A, the FAM counts enhance with the increase of FEN1 cleavage temperature from 50 °C to 65 °C, followed by decrease beyond the temperature of 65 °C. Therefore, 65 °C is selected for the optimal temperature of FEN1 cleavage. As shown in Fig. S4B, the FAM counts enhance with the FEN1 reaction time from 5 to 30 min, and reach a plateau at 30 min. Therefore, 30 min is selected as the optimal time of FEN1 cleavage reaction.

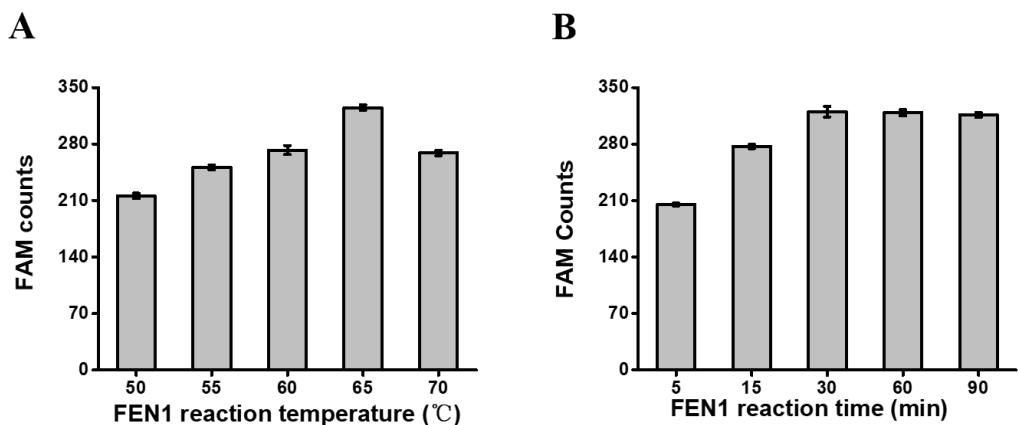


**Fig. S4** (A) Variance of the FAM counts with the FEN1 reaction temperature. (B) Variance of the FAM counts with the FEN1 reaction time. The amount of FEN1 is 16 U. Error bar represents the standard deviation of three independent experiments.

## 2.5 Optimization of LDR reaction temperature

The temperature of the LDR reaction is essential to the amplification efficiency.<sup>8</sup> As shown in Fig. S5, the FAM counts enhance with the increase of LDR reaction temperature from 35 °C to 45 °C, followed by the decrease beyond the temperature of 45 °C. Therefore, 45 °C is selected as the optimal temperature of LDR reaction.

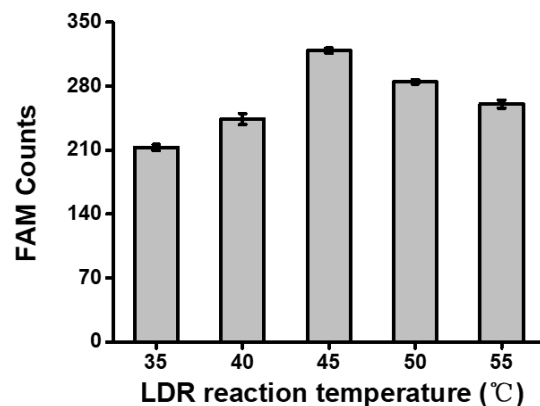


**Fig. S5** Variance of the FAM counts with the LDR reaction temperature. The amount of FEN1 is 16 U. Error bar represents the standard deviation of three independent experiments.

## 2.6 Optimization of the ratio of LDR primer/template and LDR cycle number

The ratio of LDR primer/template, and the cycle number of LDR reaction are two important factors that affect the LDR amplification efficiency. As shown in Fig. S6A, the FAM counts enhance with the ratio of LDR primer/template from 1:1 to 8:1, followed by the decrease beyond the ratio of 8:1. Therefore, 8:1 is selected as the optimal ratio of LDR primer/template of LDR reaction. As shown in Fig. S3B, the FAM counts enhance with cycle number of LDR reaction from 10 to 40, followed by the decrease beyond the cycle number of 40. Therefore, 40 is selected as the optimal cycle number in LDR reaction.

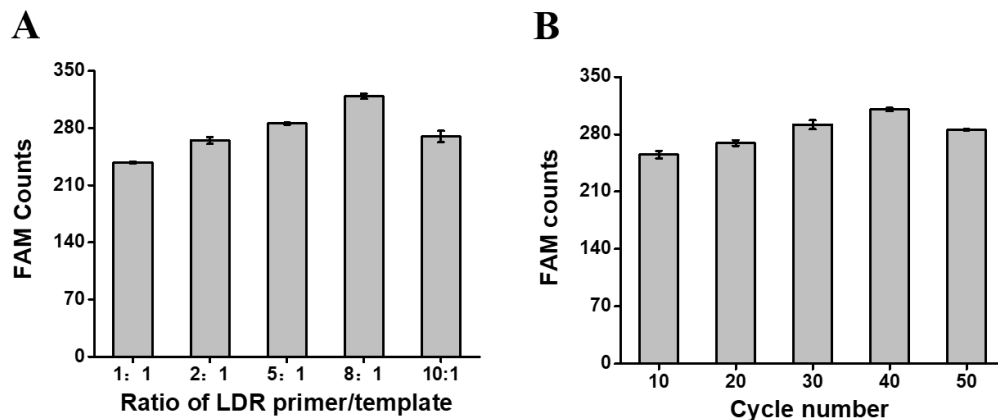


**Fig. S6** (A) Variance of the FAM counts with the ratio of LDR primer/template. (B) Variance of the FAM counts with the cycle number of LDR. The amount of FEN1 is 16 U. Error bar represents the standard deviation of three independent experiments.

## 2.7 Change of fluorescence intensity induced by different-amount FEN1

We investigated the sensitivity of the ensemble fluorescence measurement by measuring the fluorescence signals in response to different concentrations of FEN1. As shown in Figs. S7A and S7B, the fluorescence signal enhances with the increasing amount of FEN1 from  $1.6 \times 10^{-7}$  to 16 U. Moreover, the fluorescence intensity is linearly correlated with the logarithm of the FEN1 amount

in the range from  $1.6 \times 10^{-7}$  to 16 U with a correlation coefficient of 0.9927 (inset of Fig. S7B). The corresponding equation is  $F = 36479.24 + 4778.73 \lg C$ , where  $F$  is the fluorescence intensity and  $C$  is the amount of FEN1. The detection limit is evaluated to be  $6.65 \times 10^{-7}$  U based on the average signal of blank plus three times standard deviation.

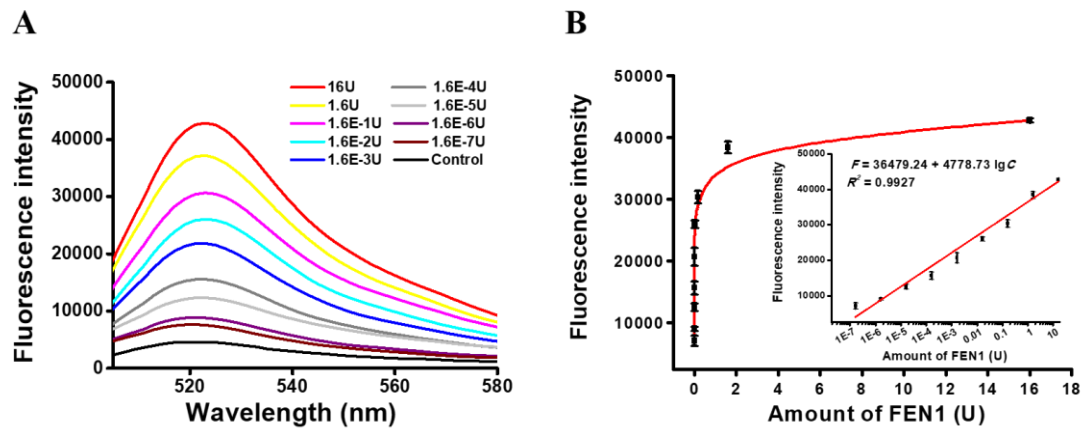


**Fig. S7** (A) Fluorescence emission spectra induced by different amounts of FEN1 in the range from  $1.6 \times 10^{-7}$  to 16 U. (B) Fluorescence intensity in response to different amounts of FEN1 from  $1.6 \times 10^{-7}$  to 16 U. Inset shows the linear relationship between fluorescence intensity and the logarithm of the FEN1 amount. Error bar represents the standard deviation of three independent experiments.

## 2.8 Detection selectivity

We further employed lambda exonuclease, exonuclease III (Exo III), bovine serum albumin (BSA), T4 DNA ligase as the interferences to evaluate the specificity of this biosensor (Fig. 3C). T4 DNA ligase catalyzes the formation of a phosphodiester bond between juxtaposed 5' phosphate and 3' hydroxyl termini in duplex DNA or RNA<sup>9</sup>. Exo III catalyzes the removal of nucleotides from dsDNA in the 3' to 5' direction<sup>10</sup>. Lambda exonuclease catalyzes the removal of nucleotides from 5'-phosphorylated dsDNA in the 5' to 3' direction<sup>11</sup>. BSA is an irrelevant protein with no cleavage activity. Weak fluorescence signals are obtained in response to lambda exonuclease (Fig. 3C, green color), Exo III (Fig. 3C, blue color), BSA (Fig. 3C, pink color), and T4 DNA ligase (Fig. 3C, yellow color), respectively, which is consistent with that generated by reaction buffer (Fig. 3C, control, grey

color). In contrast, target FEN1 induces a high FAM signal (Fig. 3C, red color). These results show that this biosensor is suitable for sensitive measurement of FEN1 with excellent specificity.

## 2.9 Original pictures of PAGE analysis

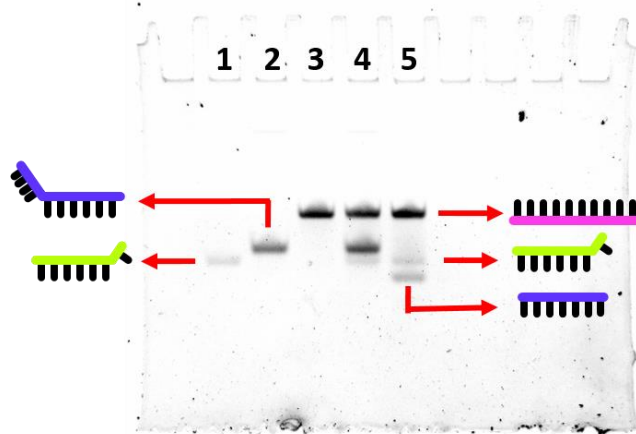


**Fig. S8** Original picture of 16% denaturing PAGE analysis of FEN1-induced cleavage of 5' flap in triplex DNA substrate. lane 1: S1; lane 2: S2; lane 3: S3; lane 4: S1 + S2 + S3; lane 5: S1 + S2 + S3 + FEN1. 16 U FEN1 was employed in the experiments.

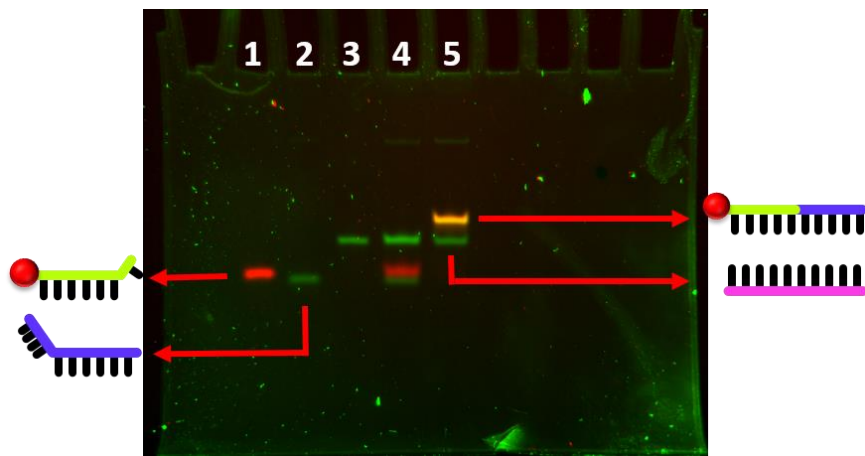


**Fig. S9** Original picture of 16% denaturing PAGE analysis of the ligation products of LDR reaction. Lane 1: S1; lane 2: S2; lane 3: S3; lane 4: S1 + S2 + S3 + DNA ligase; lane 5: S1 + S2 + S3 + DNA ligase + FEN1. 16 U FEN1 and 2.5 U DNA ligase were employed in the experiments.

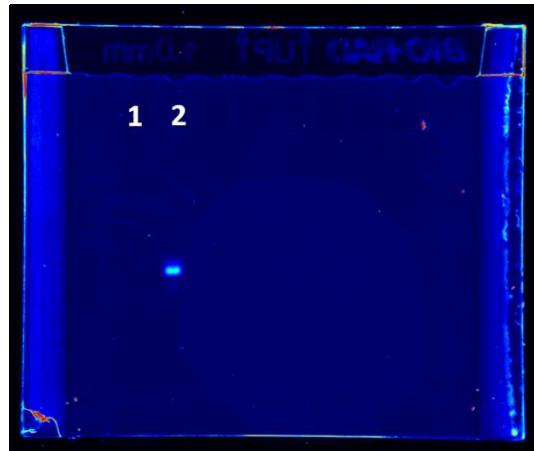


**Fig. S10** Original picture of 12% native PAGE analysis of CRISPR-Cas12a-catalyzed non-specific cleavage reaction. Lane 1, with FEN1; lane 2, without FEN1. 16 U FEN1 was employed in the experiments.

**2.10 Table S2. Comparison of the proposed method with the reported FEN1 assays**

Strategy	Signal model	Magn etic separa tion	Linear range	Real sample	LOD	Ref.
Magnetic separation-assisted enzyme-free hybridization chain reaction	cascade	Fluorescence	Yes 0.02 – 2.5 U	Cell	$1.8 \times 10^{-3}$ U	<sup>12</sup>
Nt.BstNBI-induced tandem signal amplification	UV-vis	No 0.03 – 1.5 U	No 0.01 U			<sup>13</sup>
Au nanoprobe-based assay	Fluorescence	Yes 0 – 2.0 U	Cell	$7 \times 10^{-3}$ U		<sup>14</sup>
Metal-organic framework nanoparticles-based assay	Fluorescence	No 0.05 – 2.0 U	Cell	$7 \times 10^{-3}$ U		<sup>15</sup>
Branched hybridization chain reaction amplification	ECL	Yes $6.5 \times 10^{-2} – 6.5 \times 10^3$ U/L	Cell	$2.2 \times 10^{-2}$ U/L		<sup>16</sup>
LDR- and CRISPR-Cas12a-activated dual signal amplification	Single-molecule detection	No $1 \times 10^{-7} – 9.6$ U	Cell, Tissue	$1.31 \times 10^{-8}$ U		This work

### 3 REFERENCES

1. D. C. Swarts and M. Jinek, *Mol. Cell*, 2019, **73**, 589-600.
2. (a) N. Mohammad, L. Talton, Z. Hetzler, M. Gongireddy and Q. S. Wei, *Nucleic Acids Res.*, 2023, **51**, 9894-9904; (b) W. Zhang, Y. Q. Mu, K. J. Dong, L. Zhang, B. Yan, H. Hu, Y. W. Liao, R. Zhao, W. Shu, Z. X. Ye, Y. P. Lu, C. Wan, Q. Q. Sun, L. J. Li, H. B. Wang and X. J. Xiao, *Nucleic Acids Res.*, 2022, **50**, 12674-12688.
3. Z. Y. Wang, D. L. Li, X. R. Tian, Y. Y. Li and C. Y. Zhang, *Anal. Chem.*, 2022, **94**, 11425-11432.
4. J. Xu, Z. J. Liu, Z. Zhang and T. B. Wu, *Anal. Chem.*, 2023, **95**, 10664-10669.
5. M. Karlikow, E. Amalfitano, X. L. Yang, J. Doucet, A. Chapman, P. S. Mousavi, P. Homme, P. Sutyrina, W. Chan, S. Lemak, A. F. Yakunin, A. G. Dolezal, S. Kelley, L. J. Foster, B. A. Harpur and K. Pardee, *Nat. Commun.*, 2023, **14**, 1505.
6. R. Zhao, W. Luo, Y. Wu, L. Zhang, X. Liu, J. J. Li, Y. J. Yang, L. Wang, L. J. Wang, X. L. Han, Z. Z. Wang, J. H. Zhang, K. Lv, T. M. Chen and G. M. Xie, *Nucleic Acids Res.*, 2023, **51**, 10795-10807.
7. S. R. Ranjanaware, E. K. Vesco, G. M. Shoemaker, S. S. Anekar, L. S. W. Sandoval, K. S. Meister, N. C. Macaluso, L. T. Nguyen and P. K. Jain, *Nat. Commun.*, 2023, **14**, 5409.
8. H. Y. Jia, H. L. Zhao, T. Wang, P. R. Chen, B. C. Yin and B. C. Ye, *Biosens. Bioelectron.*, 2022, **211**, 114382.
9. K. Shi, T. E. Bohl, J. Park, A. Zasada, S. Malik, S. Banerjee, V. Tran, N. Li, Z. Q. Yin, F. Kurniawan, K. Orellana and H. Aihara, *Nucleic Acids Res.*, 2018, **46**, 10474-10488.
10. Q. F. Xu and C. Y. Zhang, *Chem. Commun.*, 2014, **50**, 8047-8049.
11. S. Li, D. S. Zhao, F. F. Yang and S. F. Liu, *Chem. Commun.*, 2024, **60**, 570-573.
12. L. Zhang, X. Liu, N. Zhang, X. Liu and W. Jiang, *Sensors and Actuators B: Chemical*, 2022,

**353.**

13. H. Yang, C. Wang, E. Xu, W. Wei, Y. Liu and S. Liu, *Analytical Chemistry*, 2021, **93**, 6567-6572.
14. C. Wang, D. Zhang, Y. Tang, W. Wei, Y. Liu and S. Liu, *ACS Applied Bio Materials*, 2020, **3**, 4573-4580.
15. Y. F. Tang, W. Wei, Y. Liu and S. Q. Liu, *Anal. Chem.*, 2021, **93**, 4960-4966.
16. X. H. Li, Y. C. Huang, J. W. Chen, S. M. Zhuo, Z. Y. Lin and J. X. Chen, *Bioelectrochemistry*, 2022, **147**, 108189.